

Sensitivity and Uncertainty Analysis of Airfoil Characteristics at Low Reynolds Numbers

Shigetaka Kawai* and Akira Oyama**
Corresponding author: shigetaka@flab.isas.jaxa.jp

* Department of Aeronautics and Astronautics, University of Tokyo, Japan.

** Institute of Space and Astronautical Science, JAXA, Japan.

Abstract: The stochastic behaviors of airfoil characteristics at low Reynolds numbers under uncertain flow conditions are investigated. The potential importance of considering multiple uncertainties including the Reynolds number effect on the stochastic response of the airfoil characteristics is highlighted at low Reynolds numbers.

Keywords: Low Reynolds number airfoil, Mars airplane, Uncertainty quantification, Global sensitivity analysis.

1 Introduction

Use of airplane for Mars exploration is expected to be a new and attractive approach because the Mars airplane can explore larger regions than ground rovers and obtain more detailed information than orbiting satellites. However, the Mars airplanes are required to fly at low Reynolds numbers, and complicated flow phenomena such as laminar separation bubbles occur on the wing surface and strongly affect the aerodynamic performance of airfoils [1]. Moreover, there exist many uncertainties such as the Martian atmospheric condition that may deteriorate the airfoil performances. Hence, it is important to evaluate the effects of those uncertainties in order to enhance the success probability of the Mars exploration mission.

The objective of this study is to quantify the effects of uncertain flow conditions on the aerodynamic performances of the Ishii airfoil, which has high performance at low Reynolds number. Ishii airfoil was adopted as the main wing airfoil of the Mars airplane used in the scientific balloon experiment conducted by the Japanese Mars airplane working group [2]. These uncertainty effects on the performances of the Ishii airfoil are compared with those of the NACA0012 airfoil to discuss the difference in the stochastic behavior for the uncertain flow conditions.

2 Problem Statement

The stochastic behaviors of the aerodynamic performances are investigated under uncertain flow conditions of angle of attack α , Reynolds number based on the chord length Re , and freestream Mach number M_∞ , which follow independent uniform probability distributions. The nominal conditions of Re and M_∞ are twofold:

- Case A: $Re = 3.3 \times 10^4$ and $M_\infty = 0.28$,
- Case B: $Re = 7.0 \times 10^4$ and $M_\infty = 0.57$.

The variation intervals of Reynolds number and freestream Mach number in each case are $\pm 1.0 \times 10^4$ and ± 0.05 , respectively. The nominal conditions of α are the values at which the lift-to-drag ratio of each airfoil reaches maximum under the nominal Re and M_∞ , and the variation interval of α is ± 0.5 degree in each case.

3 Computational Setup

The non-intrusive pseudo-spectral projection method based on the polynomial chaos expansion (PCE) [3] is coupled with two-dimensional flow simulations. The contributions of each uncertain parameter to the variance of the airfoil characteristics are quantified with Sobol’s sensitivity indices [4].

3.1 Uncertainty and Sensitivity Analysis Methods

3.1.1 Stochastic Spectral Projection Method

Although the typical method for uncertainty quantification is the direct Monte Carlo simulation, the computational cost associated with the numerous analysis evaluations of outputs can be prohibitive for complicated problems such as computational fluid dynamics. The non-intrusive spectral projection method based on PCE is adopted to efficiently analyze the uncertainty.

In PCE, the expensive analysis of output $f(\boldsymbol{\xi})$ for random variable vector $\boldsymbol{\xi}$ is replaced by the approximation given as follows:

$$f(\boldsymbol{\xi}) \approx \sum_{j=0}^P \alpha_j \psi_j(\boldsymbol{\xi}), \quad (1)$$

where $\alpha_j (j = 1, \dots, P)$ are the coefficients corresponding to the polynomial basis $\psi_j (j = 1, \dots, P)$. ψ_j satisfy the following orthogonality equation:

$$\langle \psi_i \psi_j \rangle = \langle \psi_i^2 \rangle \delta_{ij}, \quad (2)$$

where δ_{ij} is Kronecker’s delta and the inner product $\langle \psi_i \psi_j \rangle$ is defined as follows:

$$\langle \psi_i \psi_j \rangle = \int_{\Omega} \psi_i \psi_j p(\boldsymbol{\xi}) d\boldsymbol{\xi}. \quad (3)$$

The weight function $p(\boldsymbol{\xi})$ is the probability density function of the random variable vector $\boldsymbol{\xi}$ and Ω is the random space.

The spectral projection method employed in this study is based on the orthogonality of the basis function ψ_j for determination of the coefficients α_j . α_j are determined from the inner product of $f(\boldsymbol{\xi})$ and ψ_j , and the inner product involves an integral in Ω . Numerical integration is then required:

$$\alpha_k = \frac{\langle f \psi_k \rangle}{\langle \psi_k^2 \rangle} = \frac{1}{\langle \psi_k^2 \rangle} \int_{\Omega} f(\boldsymbol{\xi}) \psi_k(\boldsymbol{\xi}) p(\boldsymbol{\xi}) d\boldsymbol{\xi} \approx \frac{1}{\langle \psi_k^2 \rangle} \sum_{j=1}^N w_j f(\boldsymbol{\xi}^j), \quad (4)$$

where w_j are weights and the samples of $\boldsymbol{\xi}$, $\{\boldsymbol{\xi}^j\}_{j=1}^N$ are the nodes in a quadrature scheme. Note that $f(\boldsymbol{\xi})$ is only evaluated for the nodes $\{\boldsymbol{\xi}^j\}_{j=1}^N$.

The Legendre polynomials corresponding to the uniform probability distributions of the uncertain input parameters are used as the basis of PCE. The degree of PCE is five in each stochastic dimension and the Gauss-quadrature formula extended to three dimensional integration by full tensor product is employed to calculate the PCE coefficients. Thus, the number of sampling evaluations of outputs becomes $5^3 = 125$ in each case.

3.1.2 Sobol’s Global Sensitivity Analysis

In this study, the relative contributions of each uncertain input parameter to the variance of the output of interest by Sobol’s global sensitivity analysis approach [4]. In Sobol’s approach, the total variance of the output is decomposed into the contributions of each uncertain parameter alone and of the interaction between the parameters. A brief overview of Sobol’s approach is now described. At first, any N -variate

function $f(\boldsymbol{\xi})(\boldsymbol{\xi} = (\xi_1, \dots, \xi_N))$, representing the output of interest, is decomposed as follows:

$$f(\boldsymbol{\xi}) = f_0 + \sum_{s=1}^N \sum_{i_1 < \dots < i_s} f_{i_1 \dots i_s}(\xi_{i_1}, \dots, \xi_{i_s}), \quad (5)$$

where $f_{i_1 \dots i_s}(\xi_{i_1}, \dots, \xi_{i_s})$ is determined to satisfy the following equation:

$$\int_{\Omega} f_{i_1 \dots i_s}(\xi_{i_1}, \dots, \xi_{i_s}) d\xi_k = 0 \quad \text{for } k = i_1, \dots, i_s. \quad (6)$$

Taking the variance of Eq. (5) leads to

$$V[f] = \sum_i V_i + \sum_i \sum_{i < j} V_{ij} + \dots + V_{1 \dots N}, \quad (7)$$

where $V[f]$ is the variance of $f(\boldsymbol{\xi})$ and

$$\begin{aligned} V_i &= V[E[f|\xi_i]], \\ V_{ij} &= V[E[f|\xi_i, \xi_j]] - V_i - V_j, \\ &\dots \end{aligned}$$

Here, $E[f|\xi_i]$, $E[f|\xi_i, \xi_j]$ are the conditional expectation. V_i are the variance due to the variation of only the parameter ξ_i ; $V_{ij \dots}$ are the variance due to the interaction of the parameters ξ_i, ξ_j, \dots . Dividing Eq. (7) by the total variance $V[f]$ leads to the so-called Sobol' indices defined as follows:

$$S_{i_1 \dots i_s} = \frac{V_{i_1 \dots i_s}}{V[f]}, \quad (8)$$

$$\sum_i S_i + \sum_i \sum_{i < j} S_{ij} + \dots + S_{1 \dots N} = 1. \quad (9)$$

Sobol' indices represent the relative contribution of each factor, and we can specify the input uncertain parameter with high Sobol' index as the dominant one for the output of interest.

3.2 Numerical Methods for Fluid Analysis

For the sample evaluation of the airfoil characteristics, two-dimensional flow simulations are employed because the object flows of this study does not entail the large-scale separation of the boundary layer. The governing equations are two-dimensional compressible Navier–Stokes equations. The convective terms are evaluated by 3rd-order MUSCL [5] and SHUS [6]; the viscous terms are evaluated by 2nd-order central difference scheme. For the time integration, 2nd-order ADI-SGS implicit scheme [7] is applied. In Case A, the flow field is assumed to be fully laminar so that no turbulence model is employed. This laminar simulation was shown by Lee et al. [8] to predict the airfoil characteristics with a satisfactory accuracy for the flow field without large-scale separation. On the other hand, in case B, the flow field is assumed to be turbulent, and Spalart-Allmaras turbulence model [9] is employed.

4 Results and Discussions

4.1 Deterministic Flow Fields

The typical flow fields for Case A and B are shown in Figs. 1 and 2 with the contours of streamwise velocity. As expected, the laminar separation bubbles are observed on the upper airfoil surface that entail the negative streamwise velocity region. The separation bubbles in Case A (Fig. 1) are so-called “short bubbles,” the length of which decreases along with increasing angle of attack, whereas the bubbles in Case B (Fig. 2) are so-called “long bubbles,” for which the augmentation of angle of attack increases the size of the separated region.

As for the Reynolds number effect, the laminar separation bubbles become shortened by the increasing Reynolds numbers. The Reynolds number effect is associated with the growth of the disturbance in the separated shear layer. Although the two-dimensional simulations adopted in Case A cannot capture the three-dimensional vortex structure, the increasing Reynolds number augments the two-dimensional vortices that dominate the flow fields that entail the laminar separation.

In addition to the laminar separation bubbles, trailing edge separations and onset of leading edge stall are observed in some flow fields. The trailing edge separations occur in the flow fields at low Reynolds numbers and low angles of attack in Case A. The onset of leading edge stall occur on NACA0012 airfoil at high freestream Mach numbers and high angle of attack in Case B. This onset of leading edge stall in Fig. 2 shows the effect of M_∞ that augments the separation on NACA0012 airfoil unlike the negligible M_∞ effect in Case A. On the other hand, the flow around the Ishii airfoil is less affected by Re and M_∞ than that around NACA0012 airfoil.

Thus, the patterns of flow variation due to the uncertain flow condition in Case A and B are different, and it is interesting to compare the stochastic responses and sensitivities to the uncertainties.

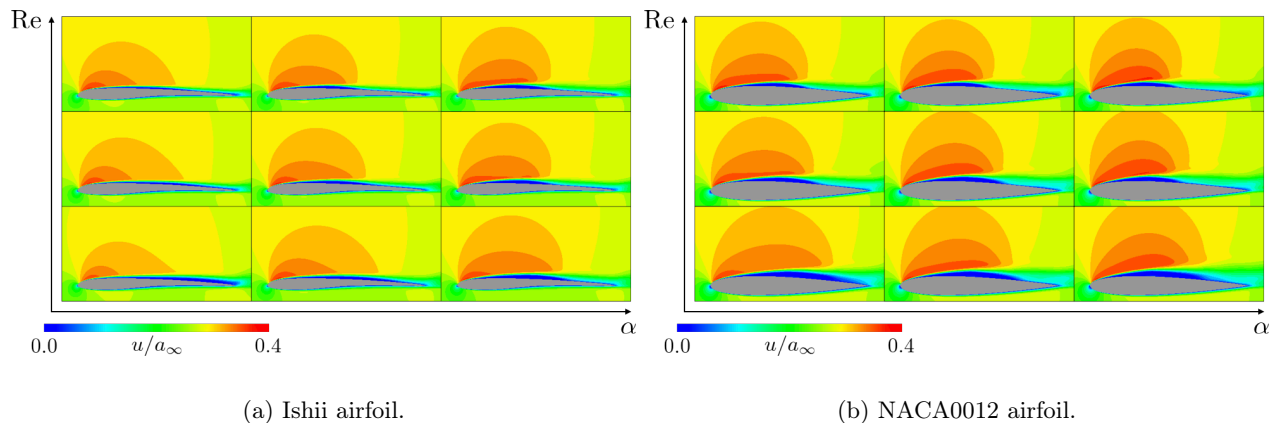


Figure 1: Time-averaged deterministic flow fields for Case A with variation of Reynolds number and angle of attack ($M_\infty = 0.28$). The contour shows the streamwise velocity fields.

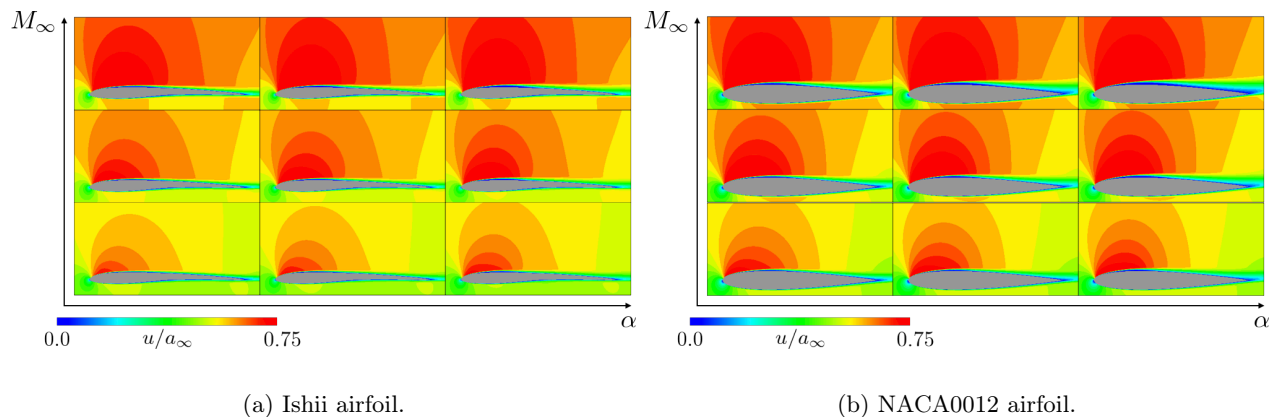


Figure 2: Time-averaged deterministic flow fields airfoil for Case B with variation of freestream Mach number and angle of attack ($Re = 7.0 \times 10^4$). The contour shows the streamwise velocity fields.

4.2 Aerodynamic Coefficients

The aerodynamic coefficients at nominal condition, statistical means, standard deviations, and Sobol' indices of the lift coefficient C_l , the drag coefficient C_d , and the lift-to-drag ratio L/D are shown for Case A and B in Tables 1 and 2, respectively. Here, the Sobol' indices S_{T_1} , S_{T_2} , and S_{T_3} represent the contributions of α , Re, and M_∞ , respectively. In addition, the coefficients of variation (COV, [%]), the ratio of the standard deviation to the statistical mean, are also shown in those tables.

Comparing the statistical means and the results at the nominal condition in Tables 1 and 2, the mean values of C_l and L/D are smaller than the values at the nominal condition; the mean value of C_d are larger than the values at the nominal condition except for that of NACA0012 airfoil in Case A. This indicates that the existence of the uncertainties in flow conditions frequently deteriorates the aerodynamic performances of airfoils. One possible reason of the smaller mean of C_d of NACA0012 airfoil in Case A is that the viscous drag is prominently reduced due to increasing Re compared with those in the other cases. This reason can be inferred from the larger Sobol' index of Re, $S_{T_2} = 0.841$ for C_d of NACA0012 airfoil in Case A.

Focusing on the standard deviations and COVs in Tables 1 and 2, it is observed that the uncertainties in flow conditions cause the aerodynamic coefficients variation of around 4 to 18 percents of the statistical mean. It should be noted that the stochastic responses to the uncertainties are different according to the nominal conditions and airfoils. From the point of view of the standard deviations, the uncertainties in flow conditions have large impacts on C_l of Ishii airfoil and C_d of NACA0012 airfoil in both Cases A and B. Comparing Cases A and B, the standard deviations of C_d of both two airfoils are larger than those in Case B. This difference in C_d is considered due to the variation of viscous drag associated with skin friction, which will be discussed later.

Let us move on to discussions on the Sobol's sensitivity indices. The higher Sobol' indices represent the larger contributions to the statistical variance of output. As an overview, the Sobol' indices of angle of attack (S_{T_1}) and Reynolds number (S_{T_2}) are large in Case A, while those of angle of attack (S_{T_1}) and Mach number (S_{T_3}) are large in Case B. In both Cases A and B, S_{T_1} of Ishii airfoil are quite large ($S_{T_1} \approx 0.8$). This large S_{T_1} means that the effect of uncertain α is dominant for C_l , and may support the deduction in the report by Anyoji et al. [2] that one possible reason for approximately 30% difference in the lift coefficient between the flight test data and experimental data is the reduction of angle of attack due to the aeroelastic deformation. As for C_d of Ishii airfoil, S_{T_2} and S_{T_3} are additionally dominant in Cases A and B, respectively. On the other hand, C_l and C_d of NACA0012 airfoil are mainly affected by Re and M_∞ in Case A and B, respectively, rather than α . Therefore, the ways of uncertain flow condition effects are different according to the airfoil shape, and it can be stated that Ishii airfoil shows a robust performance against the uncertainties on Re and M_∞ .

Table 1: Statistical data of aerodynamic coefficients for Case A.

(a) Ishii airfoil.

	Nominal	Mean	Standard Deviation	COV[%]	S_{T_1}	S_{T_2}	S_{T_3}
C_l	0.565	0.559	0.0370	6.63	0.811	0.090	0.184
C_d	2.99e-2	3.12e-2	0.391e-2	12.54	0.508	0.460	0.062
L/D	18.88	18.11	1.692	9.34	0.316	0.804	0.087

(b) NACA0012 airfoil.

	Nominal	Mean	Standard Deviation	COV[%]	S_{T_1}	S_{T_2}	S_{T_3}
C_l	0.582	0.567	0.0246	4.34	0.277	0.724	0.118
C_d	5.06e-2	5.05e-2	0.627e-2	12.40	0.159	0.841	0.0713
L/D	11.49	11.35	0.964	8.49	0.149	0.863	0.0732

Table 2: Statistical data of aerodynamic coefficients for Case B.

(a) Ishii airfoil.

	Nominal	Mean	Standard Deviation	COV[%]	S_{T1}	S_{T2}	S_{T3}
C_l	0.588	0.588	0.0402	6.83	0.849	0.0069	0.145
C_d	$2.04e-2$	$2.11e-2$	$0.254e-2$	12.03	0.518	0.0773	0.430
L/D	28.44	28.02	1.836	6.55	0.128	0.328	0.577

(b) NACA0012 airfoil.

	Nominal	Mean	Standard Deviation	COV[%]	S_{T1}	S_{T2}	S_{T3}
C_l	0.601	0.587	0.0234	3.98	0.339	0.295	0.613
C_d	$2.91e-2$	$3.03e-2$	$0.534e-2$	17.64	0.313	0.151	0.560
L/D	20.66	20.02	3.594	17.96	0.178	0.194	0.638

4.3 Surface Pressure Distribution and Skin Friction Coefficient

Figure 3 shows PDFs of surface pressure C_p at $x/c = 0.6$ in Case A. C_p PDF of Ishii airfoil in Fig. 3a exhibits a double peak, whereas that of NACA0012 airfoil in Fig. 3b does not. The existence of such a bifurcation is due to the flow transition from the trailing edge separation to the laminar separation bubble. The higher and lower peak correspond to the flows with trailing edge separation and laminar separation bubble, respectively. Accordingly, C_p distribution around Ishii airfoil abruptly change in this transition. On the other hand, in Fig. 3b, only the peak corresponding to the flow with laminar separation bubble is dominant. From this difference, the abrupt change of C_p distribution may cause the aforementioned large standard deviation of C_l of Ishii airfoil. Additionally, it is interesting that such double peak in PDF of output quantity is observed in a stochastic aerodynamic problem without any shock waves.

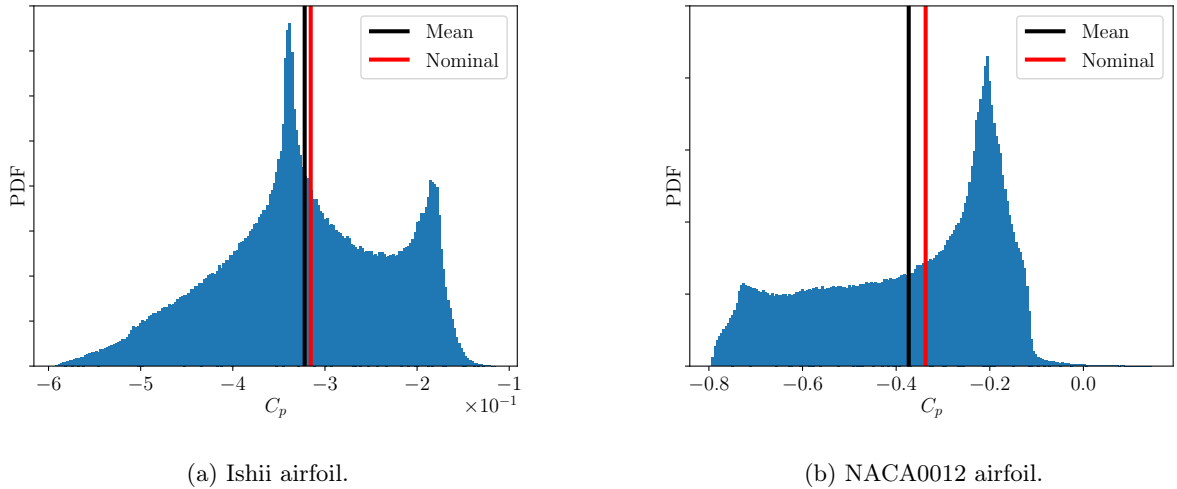


Figure 3: Probability density function of surface pressure at $x/c = 0.6$ in Case A.

Figure 4 shows the 95% confidence intervals (95CI) and statistics of the skin friction coefficient C_f for Case B. From C_f distribution, the separation and reattachment points can be estimated as the points at which C_f changes from positive to negative and from negative to positive, respectively. Comparing the skin friction coefficients of two airfoils, the 95CI errorbars of NACA0012 airfoil are laid across the line $C_f = 0$ in the region of $0.6 \leq x/c \leq 1.0$, while those of Ishii airfoil are not. This difference reflects the occurrence of

the leading edge stall observed in the flow around NACA0012 airfoil at high α and at high M_∞ in Case B, as discussed in Sec. 4.1, and can be associated with the large C_d variance of NACA0012.

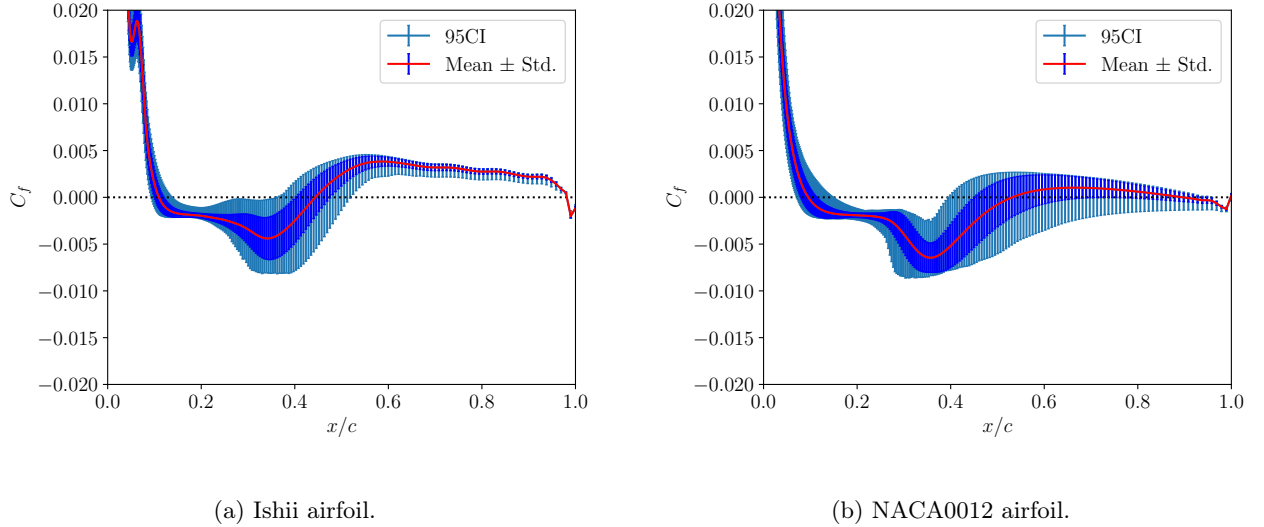


Figure 4: Statistics of skin friction coefficient in Case B.

5 Conclusions

In this study, the effects of the uncertainty in flow conditions on the airfoil characteristics at low Reynolds numbers were quantified. Ishii and NACA0012 airfoils were analyzed and compared in the stochastic response. The nominal flow condition set in this study is twofold: the steady gliding and the turbulent flow conditions. The statistical mean and standard deviation were evaluated by coupling stochastic spectral projection method with the two-dimensional flow simulations, and the relative contributions of each factor to the variance were computed by Sobol’s global sensitivity analysis.

As a result, Ishii airfoil is more sensitive to the uncertain flow conditions in lift coefficient than NACA0012 airfoil, whereas Ishii airfoil is less sensitive in drag coefficient than NACA0012 airfoil. This high sensitivity in lift of Ishii airfoil is because of the flow structure transition from a trailing edge separation to reattachment, i.e., laminar separation bubbles, on the airfoil surface. However, the sensitivity indices show that the effect on lift coefficient of Ishii airfoil is mainly due to the variation of angle of attack, rather than Reynolds number and freestream Mach number. It can be stated, therefore, Ishii airfoil achieves the robust aerodynamic design against uncertain atmospheric conditions if we are careful to the uncertainty associated with angle of attack.

References

- [1] M. O’Meara and T. Mueller. Laminar separation bubble characteristics on an airfoil at low Reynolds numbers. *AIAA Journal*, 25(8): 1033–1041, 1987.
- [2] M. Anyoji, M. Okamoto, K. Fujita, H. Nagai and A. Oyama. Evaluation of aerodynamic performance of mars airplane in scientific balloon experiment. *Fluid Mechanics Research International Journal*, 1(3), 2017.
- [3] D. Xiu and G. Karniadakis. The Wiener-Askey polynomial chaos for stochastic differential equations. *SIAM Journal on Scientific Computing*, 24(2): 619–644, 2002.
- [4] I. Sobol’. Global sensitivity indices for nonlinear mathematical models and their Monte Carlo estimates. *Mathematics and Computers in Simulation*, 55: 271–280, 2001.
- [5] B. van Leer. Toward the ultimate conservative difference scheme. 5, A second-order sequel to Godunov’s method. *Journal of Computational Physics*, 32: 101–136, 1979

- [6] E. Shima and T. Jounouchi. Role of CFD in aeronautical engineering (No. 14) —AUSM type upwind schemes—. *The 14th NAL Symposium on Aircraft Computational Aerodynamics*, 1997.
- [7] H. Nishida and T. Nonomura. ADI-SGS scheme on ideal magnetohydrodynamics. *Journal of Computational Physics*, 228: 3182–3188, 2009.
- [8] D. Lee, T. Nonomura, A. Oyama and K. Fujii. Comparison of numerical methods evaluating airfoil aerodynamic characteristics at low Reynolds number. *Journal of Aircraft*, 52(1): 296–306, 2015.
- [9] P. Spalart and S. Allmaras. A one-equation turbulence model for aerodynamic flows. *AIAA 1992-439*, 1992.